Supporting Information

The intrinsic hydrogen evolution performance of 2D molybdenum carbide

Yuqiao Wang[a], Wenting Hong [a,b], Chuangyong Jian [a,b], Xu He [a], Qian Cai [a] and Wei Liu *[a,c]

[a.] CAS Key Laboratory of Design and Assembly of Functional Nanostructures, Fujian Provincial Key Laboratory of Nanomaterial, Fujian Institute of Research on the Structure of Matter, Chinese Academy of Sciences, Fuzhou, Fujian, 350002, China

[b.] University of Chinese Academy of Sciences, Beijing, 100049, China

[c.] *Fujian Provincial Key Laboratory of Nanomaterials, Fujian Institute of Research on the Structure of Matter, Chinese Academy of Sciences, Fuzhou, 350002, China*

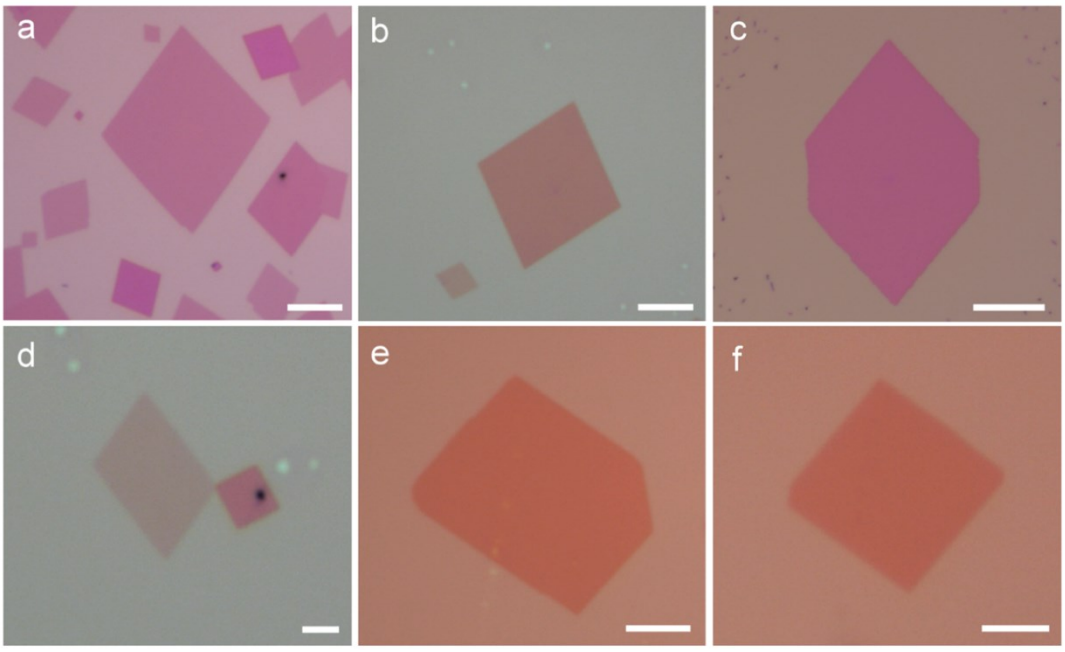

Figure S1. OM images of MoO_2 crystals with different shapes. (a) OM image of rhombic and parallelogram-type and pentagonal MoO_2 flakes, (b) rhombus, (c) hexagon, (d) parallelogram, (e) pentagon, and (f) rectangle. Scale bars are 10 μm.

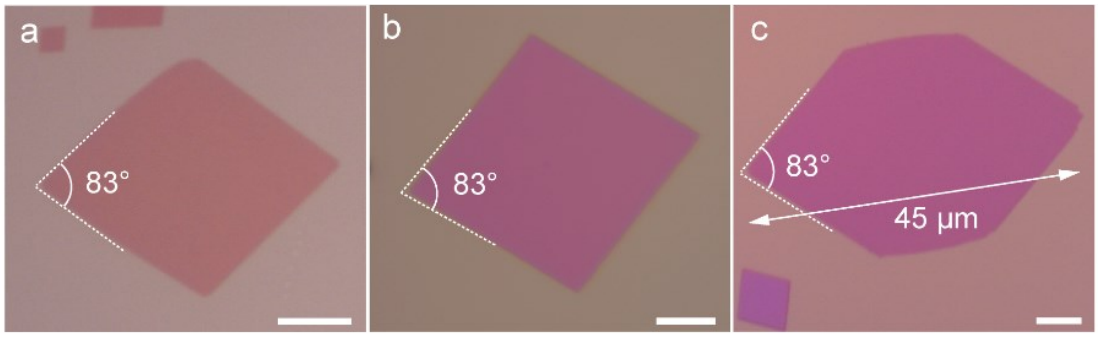

Figure S2. Thickness tunable growth of 2D MoO_2 crystals with varying growth temperature. (a－c) Optical microscopy (OM) images of rhombic and hexagonal MoO_2 flakes on the SiO_2/Si substrate at increasing temperatures of ~790°C, ~810°C, ~830 °C, respectively. The acute angle of rhombic and hexagonal MoO_2 flakes is 83°. Scale bars: 5 μm.

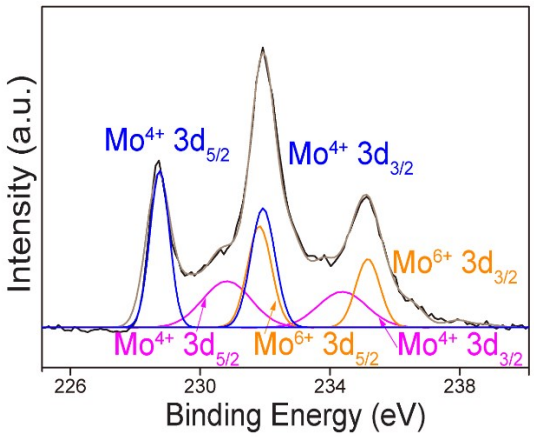

Figure S3. XPS results of Mo 3d regions of the synthesized MoO_2 flakes.

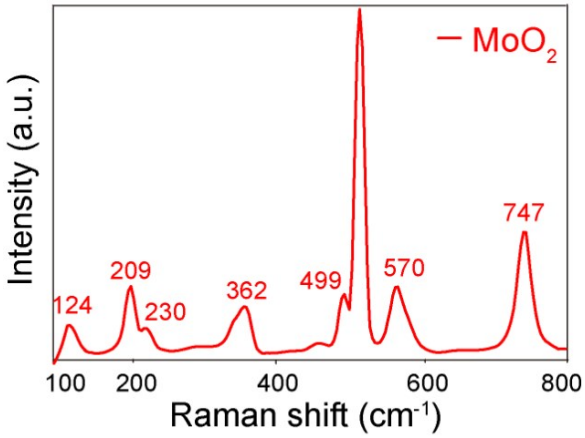

Figure S4. Raman spectra of the synthesized MoO_2 flakes.

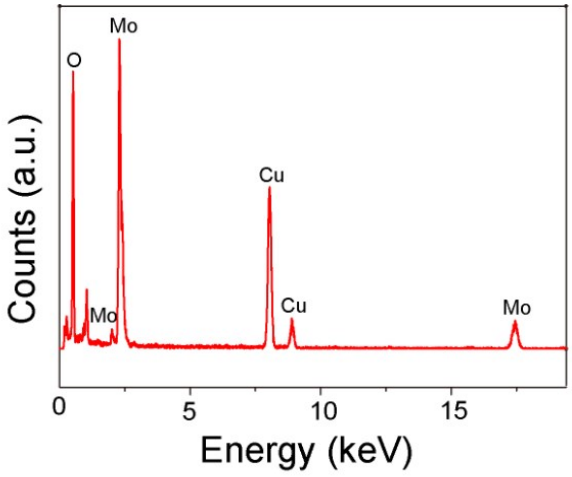

Figure S5. The energy dispersive spectrometry (EDS) analysis of the synthesized MoO_2 flakes.

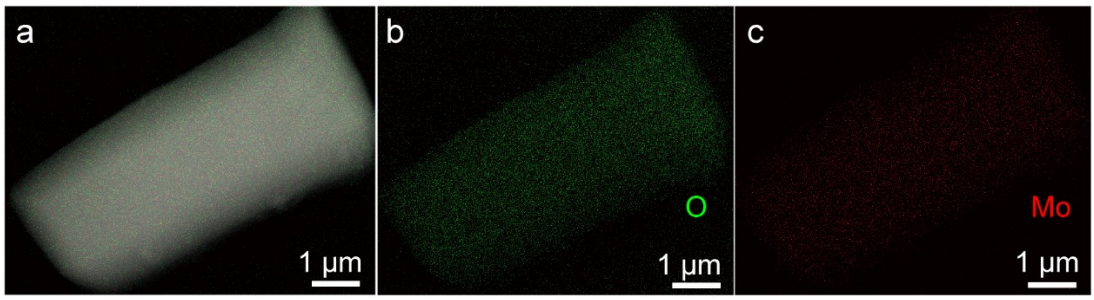

Figure S6. (a) High-angle annular dark-field scanning transmission electron microscopy image of a MoO_2 flake. (b, c) EDS mapping images of O and Mo for a MoO_2 flake achieved on a STEM grid, respectively.

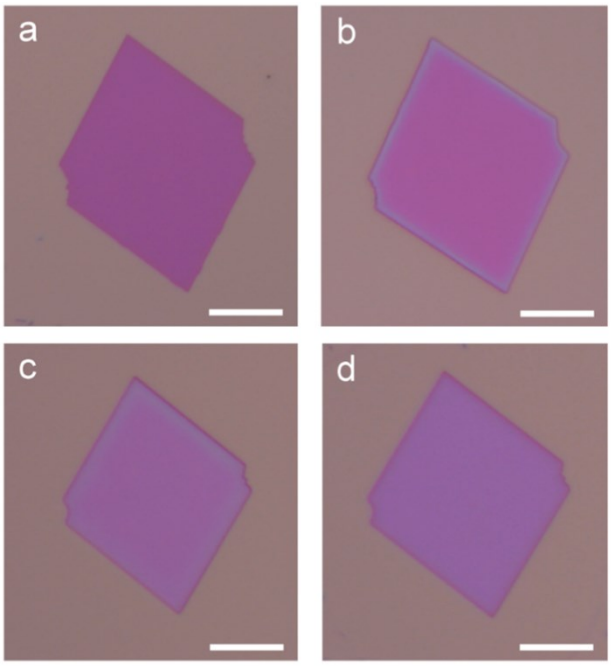

Figure S7. (a) Optical microscopy (OM) image of hexagonal MoO_2 flakes on the SiO_2/Si substrate. (b) OM images of the MoO_2/Mo_2C lateral hybrid structure and Mo_2C flakes grown at increasing carbonization time of ~10 min, ~15 min, ~40 min, respectively. The Mo_2C ratio of b, c and d is approximate ~15%, ~35%, ~100%, respectively. Red, pink regions correspond to MoO_2, Mo_2C, respectively. Scale bars: 5 μm.

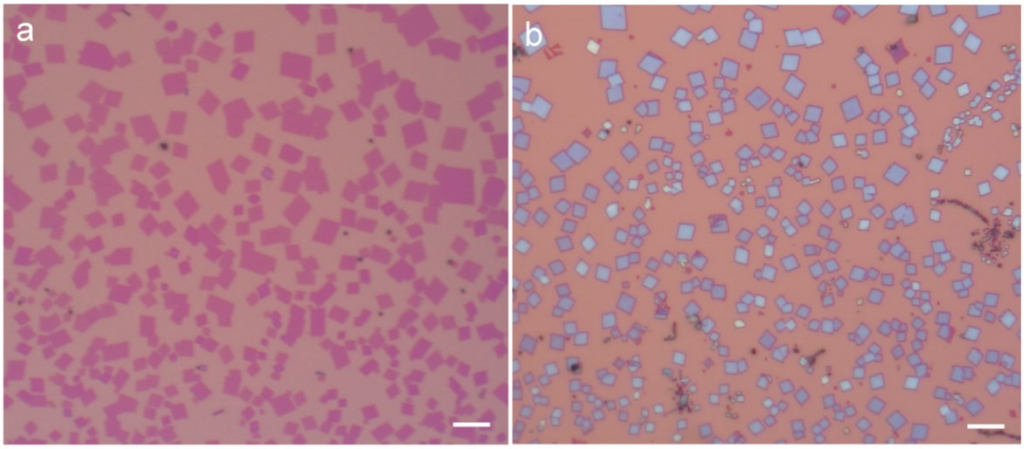

Figure S8. (a) Optical microscopy (OM) image of MoO_2 flakes on the SiO_2/Si substrate. (b) Optical microscopy (OM) image of the Mo_2C flakes on the SiO_2/Si substrate. Scale bars: 10 μm.

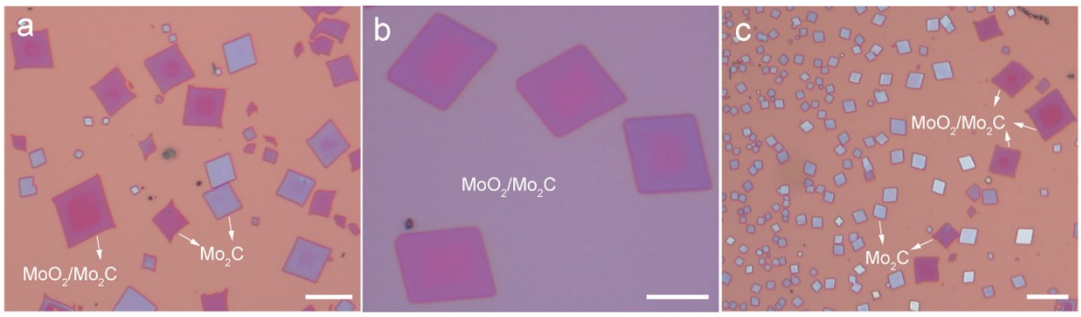

Figure S9. (a-c) Optical microscopy (OM) image of MoO_2/Mo_2C lateral hybrid structure and Mo_2C flakes grown at increasing carbonization time of ~15 min. The smaller the lateral dimension of MoO_2 flakes, the easier it is to be carbonized. Scale bars: 10 μm.

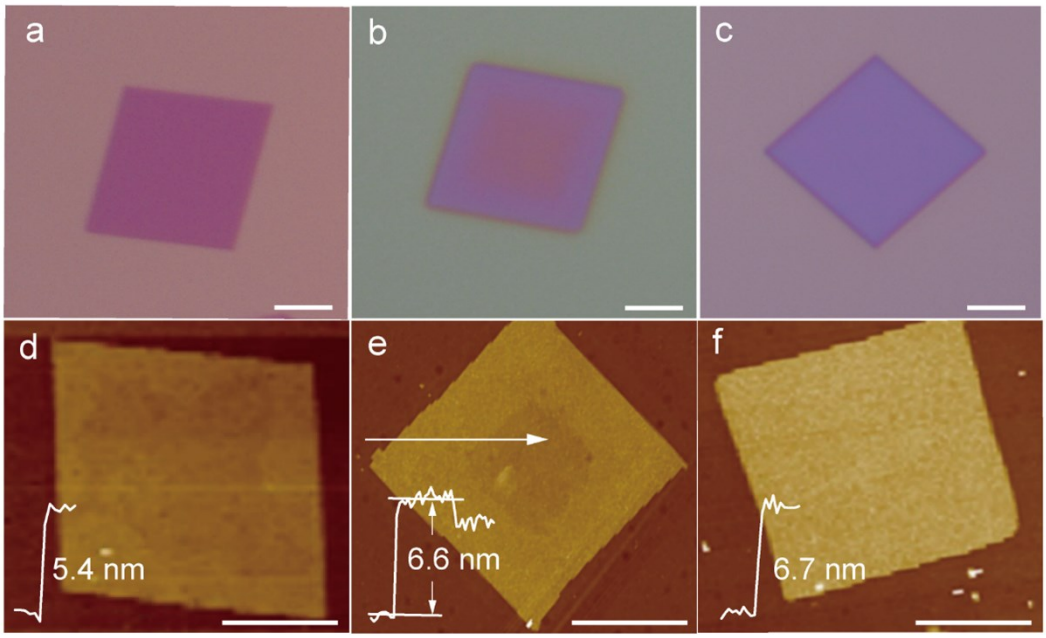

Figure S10. (a-c) Optical microscopy (OM) images of MoO_2, MoO_2/Mo_2C lateral hybrid structure and fully converted Mo_2C flakes on the SiO_2/Si substrate. (d) The corresponding atomic force microscopy (AFM) image of MoO_2 flake in (b). (e) AFM image of MoO_2/Mo_2C lateral hybrid structure in (c). Inset is the height profile along the white arrow. (f) AFM image of fully converted α-Mo_2C flake in (d). Scale bars: 5 μm.

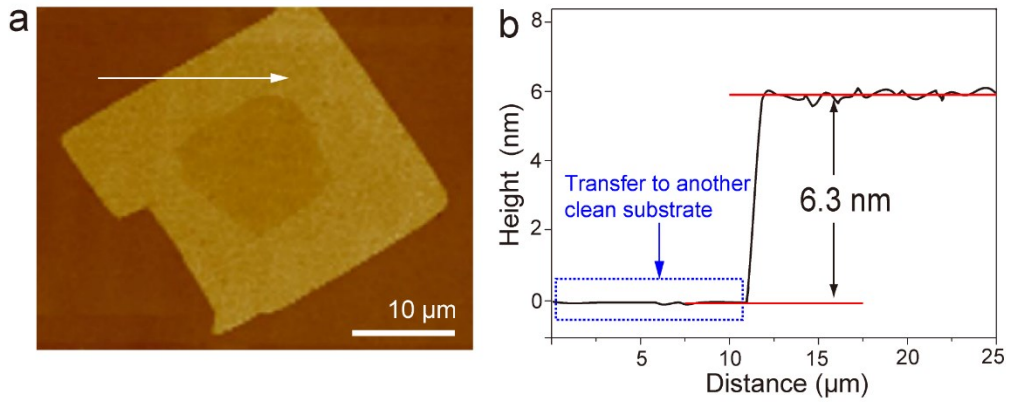

Figure S11. (a) OM image of the MoO_2/Mo_2C lateral hybrid structure is transferred to another clean SiO_2/Si substrate to eliminate the influence of the roughness of the SiO_2/Si substrate. (b) The corresponding height profile along the white arrow in (a).

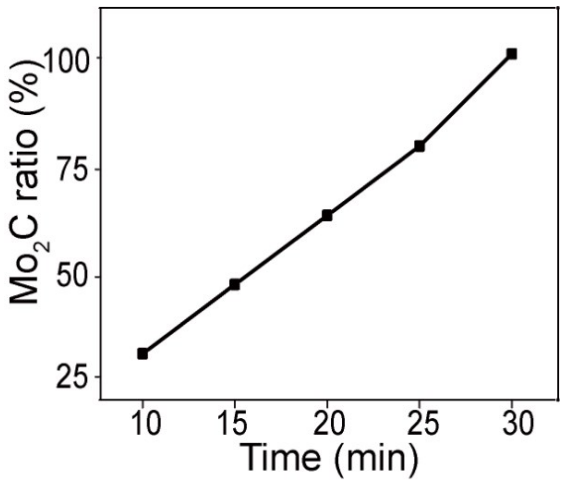

Figure S12. The ratio of Mo_2C at different thermal annealing time.

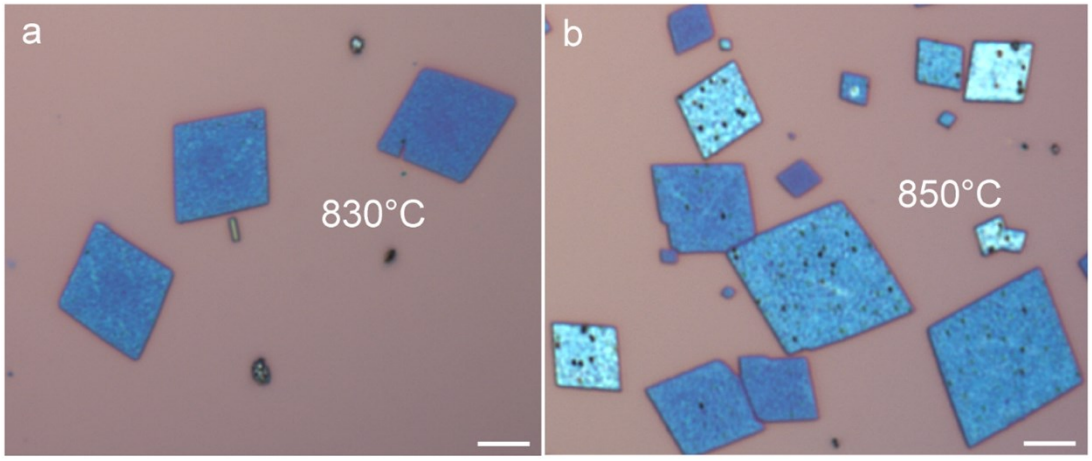

Figure S13. (a,b) OM images of the Mo_2C flakes synthesized at 830 °C and 850°C, respectively, showing rough surfaces and substantial morphological degradation.

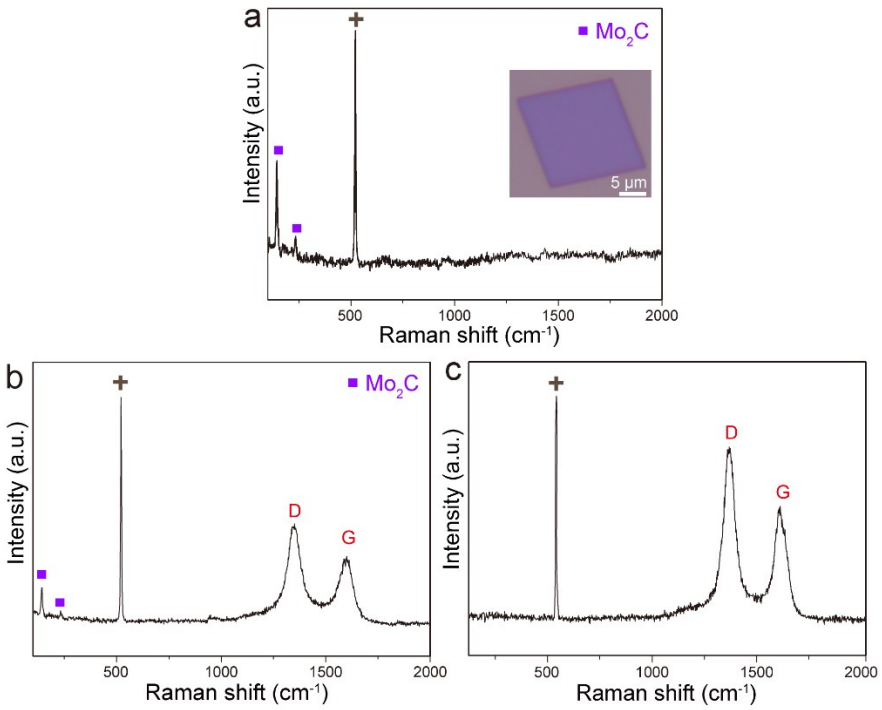

Figure S14. (a-c) Raman spectra of the synthesized Mo_2C at increasing carbonization time of ~40 min, ~50 min, ~60 min, respectively (Carbonization temperature is 800 °C). Inset in (a): The corresponding OM image of the Mo_2C flake. When the calcination time is ~40 min at 800°C, no other peaks are observed from the wide range of Raman shifts, such as the D (~1350 cm^{-1}) or G (~1595 cm^{-1}) mode of graphitic carbon. As the calcination time increases, two distinct D and G modes peaks are observed. The grey cross represents the Raman peak of Si.

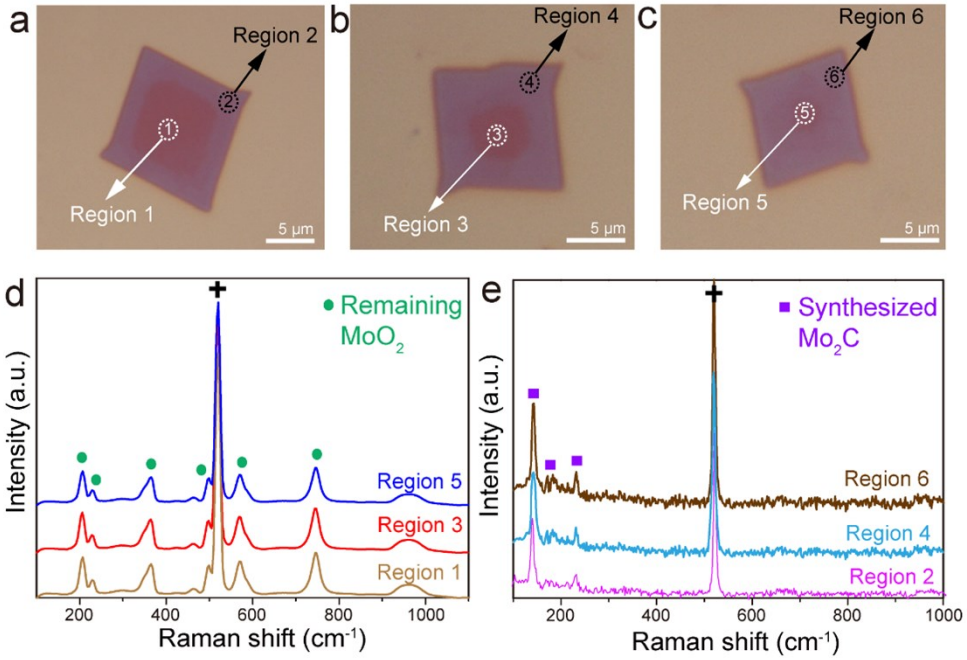

Figure S15. (a-c) OM images of MoO_2/Mo_2C lateral hybrid structure. The corresponding Mo_2C to initial MoO_2 size ratio is approximately 50%, 65%, 80%, respectively. (d, e) The corresponding Raman Spectra of the remaining MoO_2 and the synthesized Mo_2C in (a-c). The black cross represents the Raman peak of Si.

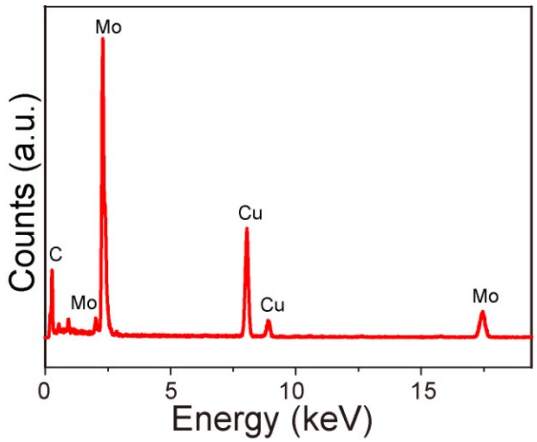

Figure S16. The EDS analysis of the Mo_2C flakes synthesized on the SiO_2/Si substrate.

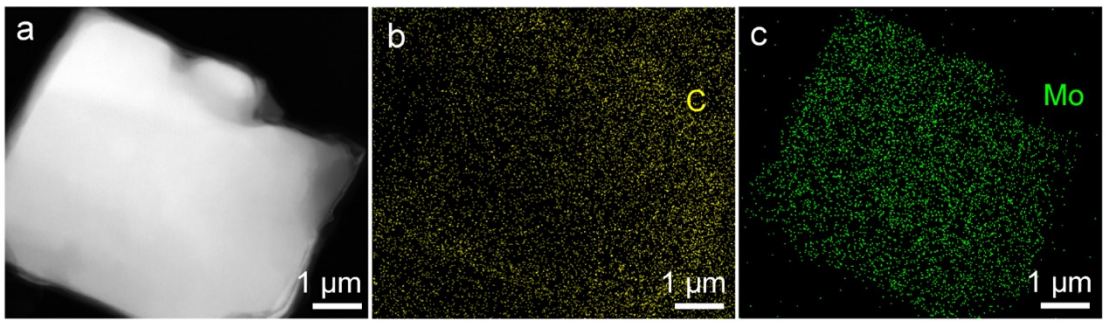

Figure S17. (a) High-angle annular dark-field scanning transmission electron microscopy image of a Mo_2C flake. (b, c) EDS mapping images of C and Mo for a Mo_2C flake achieved on a STEM grid, respectively.

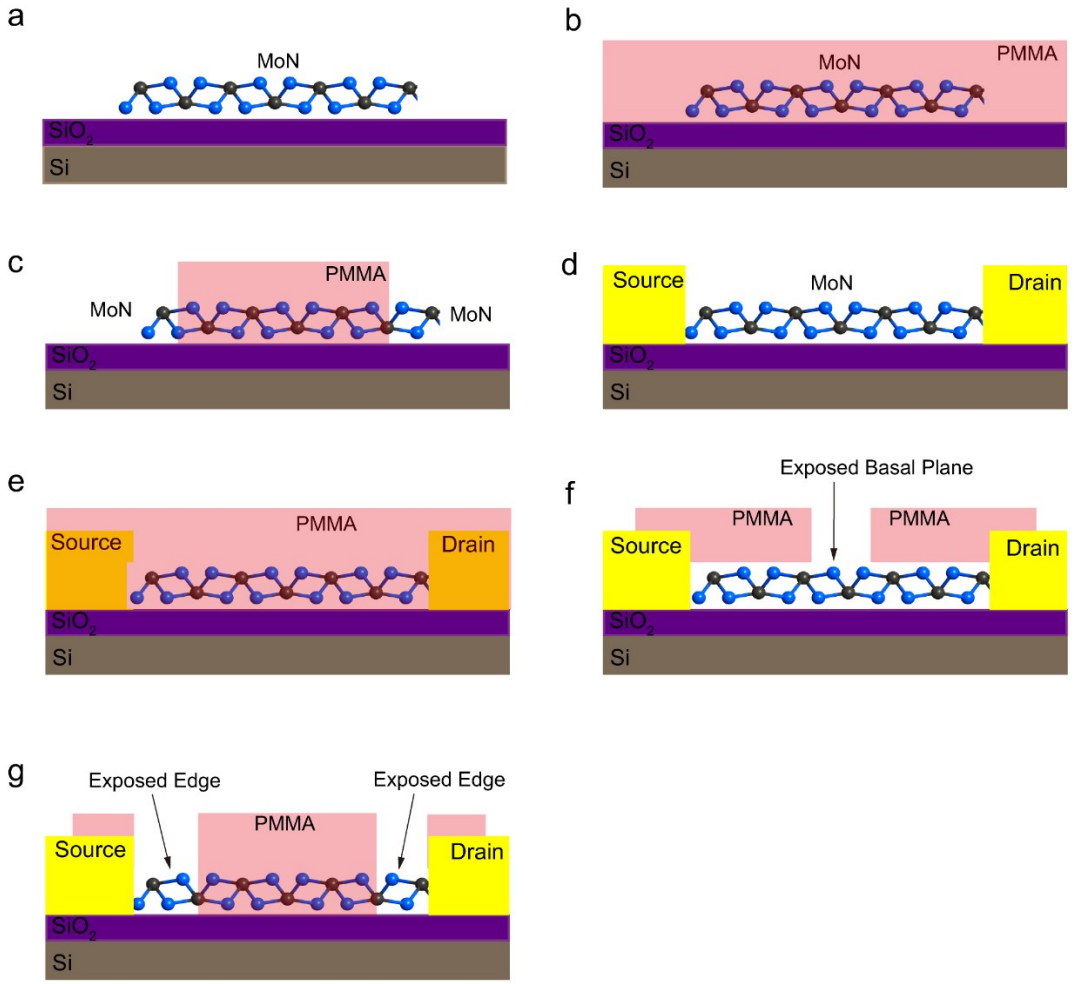

Figure S18. Illustrations displaying the EBL manufacture processes of electrochemical microcell devices setup. (a) The Mo_2C flakes are transferred on the SiO_2/Si substrate. (b) SiO_2/Si substrate was covered with PMMA. (c) Electrodes patterns are defined by EBL. (d) Cr/Au electrodes deposited to contact selected individual nanosheets via thermal evaporation. (e) The microcell setup is covered with PMMA again. (f,g) Finally step of EBL to define windows on (f) only the exposed basal plane (while covering the edges) or (g) only the exposed edges (while covering the basal plane) and electrodes.

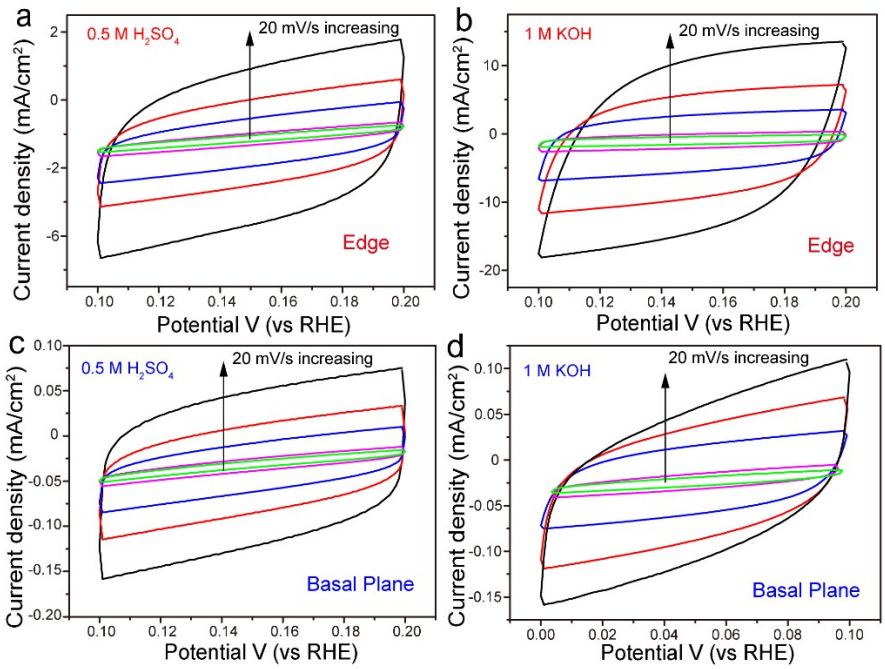

Figure S19. (a-d) Electrochemical cyclic voltammetry (CV) tests on edge and basal plane of Mo_2C with different rates from 10 to 80 mV/s in the potential range of 0.10 ~ 0.20 V in 0.5 M H_2SO_4 and 1 M KOH.

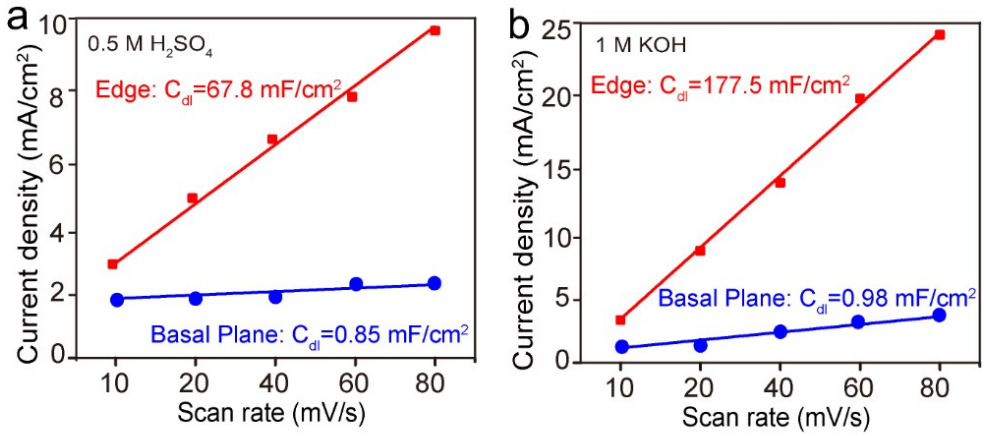

Figure S20. (a, b) C_{dl} measurements for determining electrochemically active surface areas of basal plane and edge of Mo_2C in 0.5 M H_2SO_4 and 1 M KOH.

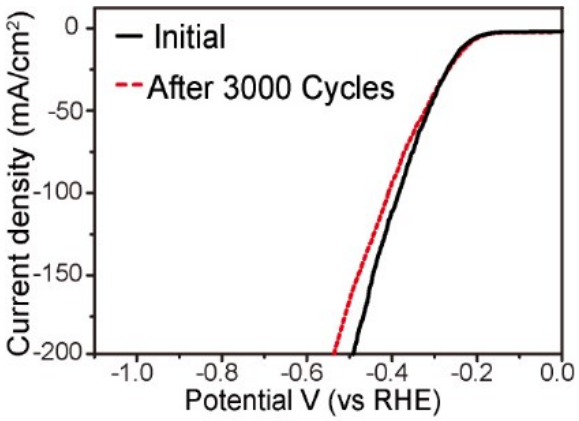

Figure S21. Long-term stability test for the 2D Mo_2C nanosheet. The polarization curves were recorded at a scan rate of 5 mV s^{-1} after 3000 potential cycles in 1 M KOH.

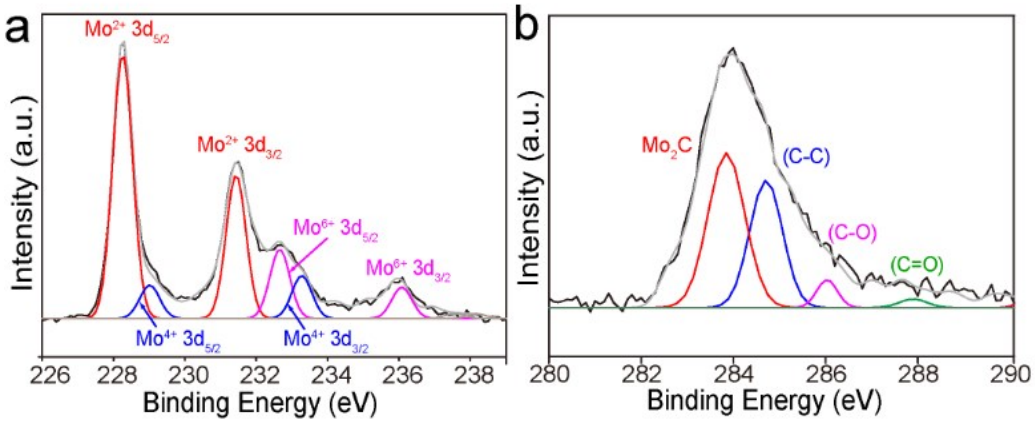

Figure S22. XPS spectra of (a) Mo 3d, (b) C 1s for 2D Mo_2C nanosheet after stability test for HER.

Table S1. A comparison of the HER parameters of the 2D Mo_2C in this work with various 2D samples and other state-of-the-art Mo_2C-based catalysts.

Materials	Substrates	Electrolytes	η (mV) (j=10 mA/cm^2)	Tafel Slope (mV/dec)	Active Site	Ref.
Mo_2C	SiO_2/Si	0.5 M H_2SO_4	281	54.4	Edge	This work
		1.0 M KOH	168	35.2		
1T-MoS_2	SiO_2/Si	0.5 M H_2SO_4	~200	~40	Edge oxidation	1
1T-MoS_2	graphite	0.5 M H_2SO_4	187	43	Edge	2
Monolayer 2H-MoS_2	Au	0.5 M H_2SO_4	170	60	S-vacancy and strain	3
$3Co_{Mo}$–V_s	SiO_2/Si	0.5 M H_2SO_4	75	57	in-plane domain	4
MoS_2/graphene	SiO_2/Si	0.5 M H_2SO_4	~200	54	grain boundaries	5
Mo SAs/ML-MoS_2	SiO_2/Si	0.5 M H_2SO_4	~107	36.4	unsaturate-d Mo SAs	6
		1.0 M KOH	~209	35.1		
Monolayer MoS_2	Glass carbon (GC)	0.5 M H_2SO_4	—	~140	Edge	7
Monolayer MoS_2	Au	0.5 M H_2SO_4	~200	61-74	Edge	8
1T'-MoS_2	SiO_2/Si	0.5 M H_2SO_4	~180	100	1T' phase	9
2H-MoS_2	SiO_2/Si	0.5 M H_2SO_4	~230	~50	Sulfur vacancies	10
Monolayer 2H-MoS_2	SiO_2/Si	0.5 M H_2SO_4	~430	~116	Edge	11
Monolayer 1T'-MoS_2	SiO_2/Si	0.5 M H_2SO_4	~355	~56	1T' phase	11
Monolayer 2H-MoS_2	Au	0.5 M H_2SO_4	—	55	Edge	12
Monolayer $MoS_{2-x}O_x$	Au	0.5 M H_2SO_4	~260	67	Oxidized basal plane	13
$Re_{0.55}Mo_{0.45}S_2$	GC	0.5 M H_2SO_4	~170	56	Re-doped	14
V_{Re}–ReS_2	SiO_2/Si	0.5 M H_2SO_4	147	69	Re vacancy	15
1T-SnS_2	SiO_2/Si	0.5 M H_2SO_4	~450	96	dendritic SnS_2	16
1T-TaS_2	Au	0.5 M H_2SO_4	~205	72	1T phase	17
2H-TaS_2	Au	0.5 M H_2SO_4	65–150	33	2H phase	18
TaS_2-N_2H_4	SiO_2/Si	0.5 M H_2SO_4	~400	76	Intercalate-d flake	19
3DHP-Mo_2C	GC	0.5 M H_2SO_4	97	60	Porous framework	20
Mo_2C NP	GC	0.5 M H_2SO_4	144	55	Nanoparticle	21
		1.0 M KOH	100	65		
Mo_2C@NC	GC	0.5 M H_2SO_4	121	67	Nanodots	22
Mo_2C NT	GC	0.5 M H_2SO_4	172	62	Nanoparticle	23
		1.0 M KOH	112	55		

References

1. D. Voiry, M. Salehi, R. Silva, T. Fujita, M. Chen, T. Asefa, V. B. Shenoy, G. Eda and M. Chhowalla, *Nano Lett*, 2013, **13**, 6222-6227.
2. M. A. Lukowski, A. S. Daniel, F. Meng, A. Forticaux, L. Li and S. Jin, *Journal of the American Chemical Society*, 2013, **135**, 10274-10277.
3. H. Li, C. Tsai, A. L. Koh, L. Cai, A. W. Contryman, A. H. Fragapane, J. Zhao, H. S. Han, H. C. Manoharan, F. Abild-Pedersen, J. K. Norskov and X. Zheng, *Nat Mater*, 2016, **15**, 364.
4. Y. Zhou, J. Zhang, E. Song, J. Lin, J. Zhou, K. Suenaga, W. Zhou, Z. Liu, J. Liu, J. Lou and H. J. Fan, *Nat Commun*, 2020, **11**, 2253.
5. Y. He, P. Tang, Z. Hu, Q. He, C. Zhu, L. Wang, Q. Zeng, P. Golani, G. Gao, W. Fu, Z. Huang, C. Gao, J. Xia, X. Wang, X. Wang, C. Zhu, Q. M. Ramasse, A. Zhang, B. An, Y. Zhang, S. Marti-Sanchez, J. R. Morante, L. Wang, B. K. Tay, B. I. Yakobson, A. Trampert, H. Zhang, M. Wu, Q. J. Wang, J. Arbiol and Z. Liu, *Nat Commun*, 2020, **11**, 57.
6. Y. Luo, S. Zhang, H. Pan, S. Xiao, Z. Guo, L. Tang, U. Khan, B. F. Ding, M. Li, Z. Cai, Y. Zhao, W. Lv, Q. Feng, X. Zou, J. Lin, H. M. Cheng and B. Liu, *ACS Nano*, 2020, **14**, 767-776.
7. Y. Yu, S.-Y. Huang, Y. Li, S. N. Steinmann, W. Yang and L. Cao, *Nano Letters*, 2014, **14**, 553-558.
8. J. Shi, D. Ma, G.-F. Han, Y. Zhang, Q. Ji, T. Gao, J. Sun, X. Song, C. Li, Y. Zhang, X.-Y. Lang, Y. Zhang and Z. Liu, *Acs Nano*, 2014, **8**, 10196-10204.
9. Y. Yu, G. H. Nam, Q. He, X. J. Wu, K. Zhang, Z. Yang, J. Chen, Q. Ma, M. Zhao, Z. Liu, F. R. Ran, X. Wang, H. Li, X. Huang, B. Li, Q. Xiong, Q. Zhang, Z. Liu, L. Gu, Y. Du, W. Huang and H. Zhang, *Nat Chem*, 2018, **10**, 638-643.
10. D. Voiry, R. Fullon, J. Yang, E. S. C. de Carvalho Castro, R. Kappera, I. Bozkurt, D. Kaplan, M. J. Lagos, P. E. Batson, G. Gupta, A. D. Mohite, L. Dong, D. Er, V. B. Shenoy, T. Asefa and M. Chhowalla, *Nat Mater*, 2016, **15**, 1003-1009.
11. J. Zhang, J. Wu, H. Guo, W. Chen, J. Yuan, U. Martinez, G. Gupta, A. Mohite, P. M. Ajayan and J. Lou, *Adv Mater*, 2017, **29**.
12. T. F. Jaramillo, K. P. Jorgensen, J. Bonde, J. H. Nielsen, S. Horch and I. Chorkendorff, *Science*, 2007, **317**, 100-102.
13. J. Peto, T. Ollar, P. Vancso, Z. I. Popov, G. Z. Magda, G. Dobrik, C. Hwang, P. B. Sorokin and L. Tapaszto, *Nat Chem*, 2018, **10**, 1246-1251.
14. S. Z. Yang, Y. Gong, P. Manchanda, Y. Y. Zhang, G. Ye, S. Chen, L. Song, S. T. Pantelides, P. M. Ajayan, M. F. Chisholm and W. Zhou, *Adv Mater*, 2018, **30**, 1803477.
15. Y. Zhou, E. Song, J. Zhou, J. Lin, R. Ma, Y. Wang, W. Qiu, R. Shen, K. Suenaga, Q. Liu, J. Wang, Z. Liu and J. Liu, *ACS Nano*, 2018, **12**, 4486-4493.
16. G. Shao, X. X. Xue, X. Zhou, J. Xu, Y. Jin, S. Qi, N. Liu, H. Duan, S. Wang, S. Li, M. Ouzounian, T. S. Hu, J. Luo, S. Liu and Y. Feng, *ACS Nano*, 2019, **13**, 8265-8274.

17. Y. Huan, J. Shi, X. Zou, Y. Gong, Z. Zhang, M. Li, L. Zhao, R. Xu, S. Jiang, X. Zhou, M. Hong, C. Xie, H. Li, X. Lang, Q. Zhang, L. Gu, X. Yan and Y. Zhang, *Adv Mater*, 2018, **30**, 1705916.
18. J. Shi, X. Wang, S. Zhang, L. Xiao, Y. Huan, Y. Gong, Z. Zhang, Y. Li, X. Zhou, M. Hong, Q. Fang, Q. Zhang, X. Liu, L. Gu, Z. Liu and Y. Zhang, *Nat Commun*, 2017, **8**, 958.
19. Y. Guo, Q. Chen, A. Nie, H. Yang, W. Wang, J. Su, S. Wang, Y. Liu, S. Wang, H. Li, Z. Liu and T. Zhai, *ACS Nano*, 2020, **14**, 1635-1644.
20. H. Ang, H. Wang, B. Li, Y. Zong, X. Wang and Q. Yan, *Small*, 2016, **12**, 2859-2865.
21. Y. Huang, Q. Gong, X. Song, K. Feng, K. Nie, F. Zhao, Y. Wang, M. Zeng, J. Zhong and Y. Li, *ACS Nano*, 2016, **10**, 11337-11343.
22. H. Wang, Y. Lin, S. Liu, J. Li, L. Bu, J. Chen, X. Xiao, J.-H. Choi, L. Gao and J.-M. Lee, *Journal of Materials Chemistry A*, 2020, **8**, 7109-7116.
23. F. X. Ma, H. B. Wu, B. Y. Xia, C. Y. Xu and X. W. Lou, *Angew Chem Int Ed Engl*, 2015, **54**, 15395-15399.